Environmental fluctuations accelerate molecular evolution of thermal tolerance in a marine diatom

C.-Elisa Schaum[1*], A. Buckling[1], N. Smirnoff[2], D. Studholme[2], & G. Yvon-Durocher[1 *]

[1] Environment and Sustainability Institute, University of Exeter, Penryn Campus, Penryn, Cornwall TR10 9EZ, UK,

[2] Biosciences, College of Life and Environmental Sciences, Geoffrey Pope Building University of Exeter, Exeter, EX4 4QD, UK

*Correspondence to c.l.schaum@exeter.ac.uk or g.yvon-durocher@exeter.ac.uk

Words in summary: 150

Words in main text: 2500

Number of Figures (main text): 4

Number of Tables (main text): 0

Diatoms contribute roughly 20% of global primary production, but the factors determining their ability to adapt to global warming are unknown. Here we quantify the capacity for adaptation to warming in the marine diatom *Thalassiosira pseudonana*. We found that evolutionary rescue under severe warming was slow but adaptation to more realistic scenarios, where temperature increases were moderate or where they fluctuated between benign and severe conditions, was rapid. Adaption to warming was linked to major phenotypic changes in metabolism and elemental composition. Whole genome re-sequencing identified significant genetic divergence both among populations adapted to the different warming regimes and between the evolved and ancestral lineages. Consistent with the phenotypic changes, the most rapidly evolving genes were associated with photosynthetic, transcriptional and translational processes. These results demonstrate that evolution of thermal tolerance in marine diatoms can be rapid, particularly in fluctuating environments, and is underpinned by major genomic and phenotypic divergence.

Introduction

Earth system models predict that global warming will result in significant declines in net primary production by marine phytoplankton throughout the 21st century (up to 20%)[1,2] driven by rising temperatures exceeding limits of thermal tolerance and increases in grazing and nutrient limitation in warmer, more stratified oceans[3-5]. Current models however, do not consider the potential marine phytoplankton to rapidly adapt to environmental changes associated with global warming[6-8]. Such shortcomings have unknown consequences for projected changes global ocean primary production and arise because the mechanisms that facilitate or constrain the capacity for

rapid adaptation to warming in marine phytoplankton are entirely unknown.

Here, we address this fundamental knowledge-gap by carrying out a 300-generation selection experiment, with the model marine diatom, *Thalassiosira pseudonana*, to assess the potential for, and mechanisms that might facilitate rapid adaptation to warming in this globally important phytoplankton[9-11]. A key hypothesis we test is that rapidly fluctuating temperatures – an intrinsic feature of natural environments – will play a key role adaptation[12-14]. Temporary exposure to a benign environment resulting from temperature fluctuations could both accelerate adaptation to severe conditions by increasing population size (a positive demographic effect) or constrain adaptation, by relaxing selection for beneficial mutations that promote persistence in the harsh environment (a negative population genetic effect)[12,13]. Our experiment was initiated with a single clone (the ancestor), which had an upper thermal limit of 35ºC. The ancestor was then distributed among 4 experimental treatments that represent a range of warming scenarios (Fig S1 for experimental set-up): (i) a control at 22ºC, which was the long-term culture temperature; (ii) moderate warming at 26ºC; (iii) severe warming at 32ºC and (iv) a fluctuating thermal regime, which cycled between 22 and 32ºC every 3-4 generations. To understand the mechanisms that set the limits of thermal tolerance in marine diatoms and quantify the capacity for adaptation beyond present limits, we re-sequenced the genomes, measured growth rate, photosynthesis, respiration and elemental composition in the ancestor and evolved lineages after approximately 300 generations of selection.

Results & Discussion

Evolution of thermal tolerance

Trajectories of population growth rate (μ, d^{-1}) over the course of the selection experiment differed substantially between the selection regimes (Fig. 1; Table S1-Table S3). In the control lineages, growth rates increased gradually, presumably reflecting continual laboratory adaptation. However, trajectories of growth rate in the warming treatments were markedly different from the control and one another. Lineages selected under severe warming (32ºC) exhibited a characteristic pattern of 'evolutionary rescue'[14-17] . After an initial increase in the first 3 weeks of the experiment, growth rates declined in the 32ºC environment and remained very low (0.24 ± 0.09) for more than one year (~ 100 generations). After approximately 100 generations, growth rates increased and were statistically indistinguishable from those in the control environment after 300 generations (0.63 ± 0.05 at 32ºC, 0.77± 0.11 at 22ºC). Under moderate warming (26ºC), and in the regime that fluctuated between 22 and 32ºC growth rate showed an immediate and sustained increase (2.1 and 1.9-fold faster than the ancestor respectively). These results yield a number of important insights that are pertinent for understanding the evolutionary dynamics of *T. pseudonana* in response to warming. First, adaptation to severe warming was slow, with evolutionary rescue taking over 1 year to restore growth rates to levels comparable with the ancestor. Second, in the fluctuating environment where populations experienced short bursts of exposure to 32ºC followed by periods in the benign (22ºC) environment, adaptation to the severe environment was rapid. Consistent with our hypothesis, lineages selected under the fluctuating regime maintained substantially larger population sizes relative to those experiencing severe warming (Fig. S2 and Table S1, S3), suggesting that temporary restoration of benign conditions increased the probability of fixing beneficial mutations required for adaptation to the severe (32ºC) environment *via* a positive demographic effect.

To assess whether adaptation to the various selection regimes changed the thermal tolerance curves in the evolved lineages, we quantified growth rates across a temperature gradient spanning 15ºC to 40ºC. Populations selected under the moderate (26ºC), severe (32ºC) and fluctuating (22ºC/32ºC) warming treatments had higher optimal growth temperatures, T_{opt}, compared to the ancestor and the control (Fig. 1B; Table S1). In the fluctuating treatments, growth rate at high temperatures was traded-off against slow growth at low temperature, suggesting that the severe environment was the dominant driver of selection. By contrast, high temperature tolerance in the moderate warming treatments appeared to incur no cost in performance at low temperature. Despite having a high T_{opt}, the lineages selected under constant severe warming had the slowest growth rates at all measurement temperatures except for 40ºC, the most extreme temperature. A key question therefore is: what mechanisms facilitated the rapid evolution of increased thermal tolerance in the lineages selected under moderate and fluctuating warming?

Increased metabolic efficiency facilitates evolution of thermal tolerance

The fraction of photosynthesis that can be allocated to growth tends to decline with warming, owing to the high temperature sensitivity of respiration relative to photosynthesis, suggesting that the upper thermal tolerance of phytoplankton reflect metabolic constraints that limit the efficiency of carbon allocation to growth at high temperature[18]. To investigate whether changes in metabolic traits could help explain the thermal tolerance curve of the ancestor and evolutionary shifts observed over the selection experiment, we measured responses of gross photosynthesis (P) and respiration (R) to acute gradients in temperature, spanning 4 to 45ºC, in

the ancestor and all evolved lineages. In contrast to previous work[18], the activation energies characterising the temperature sensitivities of *P* and *R* in the ancestor were equivalent (e.g. E_a for *P* = 1.08eV ± .0.18 s.e.m., and E_a for *R* = 1.07 ± 0.17 s.e.m.), i.e. increases in *P* and *R* up to the optima were similar (Fig. 2; Table S6-S8). Optimum temperatures for *P* were however lower than those for *R* (T_{opt} for *P*: 27 ºC ± 0.7ºC, (± s.e.m.); T_{opt} for R = 29 ºC ± 0.36ºC, (± s.e.m.)), meaning that above T_{opt} for *P*, the carbon-use efficiency (CUE = 1 – *R*/*P*; i.e., the *potential* carbon for allocation to growth) declined rapidly. The optimum temperature for growth rate (T_{opt} = 28ºC; Fig. 1B) and subsequent decreases in growth at supra-optimal temperatures coincided with declines in the CUE above T_{opt} for *P* in the ancestor, demonstrating that the temperature dependence of CUE imposes a physiological constraint that shapes the thermal tolerance curve. Thus, we hypothesize that shifts in traits that increase CUE at high temperatures should have played an important role in facilitating adaptation to warming in the evolved lineages of *T. pseudonana*.

Following 300 generations of selection, we observed substantial shifts in the temperature responses of *P* and *R*, both among treatments, as well as between the evolved lineages and the ancestor (Fig. 2; Tables S4 –S8). For both *P* and *R*, estimates of T_{opt} in the warming treatments were higher than the ancestor and control, and rates of *P* and *R* declined less abruptly at temperatures exceeding T_{opt}. Consequently, CUEs remained high at hotter temperatures in the warming treatments. The mass-specific rates of *P* and *R* normalized to a reference temperature T_c = 18ºC ($P(T_c)$ and $R(T_c)$, see Eq.6), were significantly down-regulated under moderate, severe and fluctuating warming, relative to the control treatment and the ancestor (Fig. 2 C, D, Tables S7 –S9). Rates of $R(T_c)$ also decreased more than those of $P(T_c)$, resulting in an overall increase in CUE in the lineages selected under moderate and fluctuating warming (Fig. 2E). These results

support our hypothesis of fluctuating temperatures facilitating thermal adaptation and show that changes in the traits that increase the CUE, played an important role in the evolution of elevated thermal tolerance in the treatments subjected to warming. It is notable however, that the populations experiencing severe warming had lower growth rates and lower CUEs than the lineages in the moderate and fluctuating warming treatments (Fig. 1B, Fig. 2E, Table S1 and S9, also Fig S3). This suggests that while evolutionary rescue restored growth rates to levels comparable with the control, 300 generations of selection under constant, severe warming was insufficient to evolve CUEs that facilitate growth rates comparable to populations that experienced only brief periods of severe conditions.

Changes in subcellular resource allocation

So how were the lineages selected under the moderate and fluctuating warming regimes able to achieve the shifts in metabolic efficiency that facilitated rapid adaptation to warming? Changes in temperature are known to alter optimal subcellular allocation of resources to various macromolecular classes through phenotypic plasticity (i.e. acclimation)[19-24]. Indeed, algae exposed to warming often increase their nitrogen-to-phosphorous ratios (N:P) by down-regulating the density of P-rich ribosomes, relative to N-rich proteins, owing to the increased efficiency of protein synthesis by ribosomes at higher temperatures[21-24]. We quantified cellular macromolecular composition in the ancestor and the evolved lineages to investigate the biochemical basis for the adaptive shifts in growth and metabolic efficiency, and found marked shifts in elemental composition, both among treatments and between the evolved and ancestral lineages (Fig. 3). Nutrient-use efficiency (expressed as growth rate per pg of nitrogen (N) or

phosphorous (P)), the chlorophyll-to-carbon ratio and the quantum efficiency of photosystem II (Φ_{PSII}; the proportion of the total light absorbed by PSII that is used in photochemistry) were highest in the fastest growing populations selected under moderate and fluctuating warming. We also found a positive temperature response in the N:P and C:P ratios, that was consistent, both in direction and magnitude, with the short-term acclimation responses characterised in the ancestor, confirming hypotheses[21-23] that the direction of phenotypic plasticity (acclimation) and adaptive shifts in macromolecular composition are convergent (see also Fig S4 and Fig S5, and Tables S10-S11). Together these results suggest that the greater down-regulation of $R(T_c)$ relative to $P(T_c)$, which enabled increased efficiency of C allocation to growth and facilitated rapid adaptation to moderate and fluctuating warming, were in turn tightly coupled to major adjustments in allocation to the key macromolecular classes that determine cellular composition.

Molecular evolution of thermal tolerance

To investigate whether the observed changes in fitness and phenotypes in the evolved lineages were also reflected by consistent patterns of molecular evolution, we resequenced the genomes of the ancestor and the evolved populations to determine the identity and frequency of mutations. Using only non-synonymous single nucleotide polymorphisms (SNPs), we quantified the number of sites that acquired mutations in each population relative to the ancestral reference sequence, and from allele frequencies, the genetic distance of each population from the ancestor and the genetic divergence among populations. Consistent with the fitness trajectories (Fig. 1A), all evolved populations showed significant genetic divergence from the ancestor (Fig. 4A; Table S12). The lineages selected under moderate and fluctuating warming had the greatest genetic

distance from the ancestor (Fig. 4A; Fig. S6, Table S13). Furthermore, the populations that experienced fluctuations between severe and benign conditions were significantly divergent from those experiencing constant severe warming. These results are consistent with the demographic data (Fig. 1A; Fig S2), indicating that the temporary restoration of benign conditions in the fluctuating regime accelerated rates of molecular evolution, potentially supplying mutations that were beneficial under the severe conditions. Comparing principal component analyses (PCA) based on combining all the phenotypic data, with the PCA from the non-synonymous SNPs, revealed striking similarities in the patterns of divergence among treatments (Fig. 4A,B, Figs S6, S7, Table S12, S13). These results suggest that the observed changes in metabolic traits and elemental composition that were linked to the evolution of thermal tolerance could also have a basis in some of the underlying genomic changes. To investigate this, we identified the top 20 SNPs most strongly associated with the first and second principal components. We then identified the genes (see Table S14) and protein functions (when annotated in the reference genome) associated with these SNPs. Mutations most strongly associated with the lineages selected under moderate and fluctuating warming clustered in gene families linked to photosynthetic pathways, while the populations evolved under constant severe warming showed a dominance of mutations in genes related to transcriptional and translational processes (Fig. 4C). Mutations in transcriptional and translational genes, such as the plastid RNA polymerase subunits (*rpoC* and *rpoC*2 – associated with 32ºC lineages), have been shown to be linked to stress responses in bacteria[28] and may indicate that consistent with their poor growth and physiological performance, even after 300 generations of selection, these lineages were still under severe thermal stress at 32ºC. Conversely, the overall larger genetic distances relative to the ancestor in the lineages selected under moderate and fluctuating warming, as well as the

predominance of mutations related to photosynthetic pathways, may be indicative of more fundamental metabolic rearrangements associated with the evolution of increased physiological performance at high temperatures in these populations.

Our results shed new light on the adaptive potential and evolutionary dynamics of one of the most abundant and widely distributed eukaryotic marine phytoplankton in response to warming. We found that evolutionary rescue under severe warming was slow (> 1 year), but adaptation to more realistic warming scenarios, where temperature increases were moderate or where they fluctuated between benign and severe conditions, was rapid. The fluctuating environment accelerated adaptation to severe warming because temporary restoration of benign conditions increased population size and therefore the probability of fixing beneficial mutations required for adaptation to the severe environment. Consistent with this demographic effect, the lineages selected under fluctuating warming had the greatest genetic distance from the ancestor after 300 generations, indicating accelerated rates of molecular evolution. Because our experiments were initiated with a single clone, they may in fact be conservative estimates of the evolutionary potential of the highly diverse meta-population of *T. pseudonana* in the wild[5] where adaptation will also be aided by standing genetic variation. Our results also show how rapid, adaptive shifts in thermal tolerance are linked to major phenotypic changes in metabolism and elemental composition as well as significant molecular evolution, particularly in genes associated with photosynthesis, transcription and translation processes. Because the changes in carbon-use efficiency in the warm-adapted lineages arise due to differences the temperature sensitivities of photosynthesis and respiration, which are highly conserved metabolic pathways, our work raises the prospect that at the physiological-level, the mechanisms underpinning rapid thermal adaptation could be universal across the broad diversity of phytoplankton. Our findings could

220 therefore help integrate rapid evolution into models of ocean biogeochemistry and improve
221 projections of marine primary productivity over the 21st century[1,25].

222

223 **References (1-25 main text, 25-50 methods)**

224 1. Bopp, L. *et al.* Potential impact of climate change on marine export production. *Global Biogeochem.*
225 *Cycles* **15,** 81–99 (2001).
226 2. Steinacher, M. *et al.* Projected 21st century decrease in marine productivity: a multi-model analysis.
227 *Biogeosciences* **7,** 979–1005 (2010).
228 3. López-Urrutia, Á., Martin, E. S., Harris, R. P. & Irigoien, X. Scaling the metabolic balance of the
229 oceans. *Proceedings of the National Academy of Sciences* **103,** 8739–8744 (2006).
230 4. Laufkötter, C. *et al.* Drivers and uncertainties of future global marine primary production in marine
231 ecosystem models. *Biogeosciences* **12,** 6955–6984 (2015).
232 5. Regaudie-de-Gioux, A. & Duarte, C. M. Compensation irradiance for planktonic community
233 metabolism in the ocean. *Global Biogeochem. Cycles* **24,** GB4013, doi:10.1029 /2009GB003639
234 (2010).
235 6. Reusch, T. B. H. & Boyd, P. W. Experimental Evolution Meets Marine Phytoplankton. *Evolution* **67,**
236 1849–1859 (2013).
237 7. Thomas, M. K., Kremer, C. T., Klausmeier, C. A. & Litchman, E. A Global Pattern of Thermal
238 Adaptation in Marine Phytoplankton. *Science* **338,** 1085–1088 (2012).
239 8. Schluter, L. *et al.* Adaptation of a globally important coccolithophore to ocean warming
240 and acidification. *Nature Climate Change* **4,** 1024–1030 (2014).
241 9. Field, C. B. Primary Production of the Biosphere: Integrating Terrestrial and Oceanic Components.
242 *Science* **281,** 237–240 (1998).
243 10. Falkowski, P. G. Biogeochemical Controls and Feedbacks on Ocean Primary Production. *Science*
244 **281,** 200–206 (1998).
245 11. Armbrust, E. V. The Genome of the Diatom Thalassiosira Pseudonana: Ecology, Evolution, and
246 Metabolism. *Science* **306,** 79–86 (2004).
247 12. Hao, Y.-Q., Brockhurst, M. A., Petchey, O. L. & Zhang, Q.-G. Evolutionary rescue can be impeded
248 by temporary environmental amelioration. *Ecol Lett* **18,** 892–898 (2015).
249 13. Ashander, J. & Chevin, L. M. Predicting evolutionary rescue via evolving plasticity in stochastic
250 environments. *Proceedings of the Royal Society B: Biological Sciences* **283,** 20161690 (2016).
251 14. Bell, G. Evolutionary rescue and the limits of adaptation. *Philosophical Transactions of the Royal*
252 *Society B: Biological Sciences* **368,** 20120080–20120080 (2012).
253 15. Lachapelle, J. & Bell, G. Evolutionary Rescue Of Sexual And Asexual Populations In A
254 Deteriorating Environment. *Evolution* **66,** 3508–3518 (2012).
255 16. Elena, S. F. & Lenski, R. E. Test of synergistic interactions among deleterious mutations in bacteria.
256 *Nature* **390,** 395–398 (1997).
257 17. Bell, G. & Gonzalez, A. Adaptation and Evolutionary Rescue in Metapopulations Experiencing
258 Environmental Deterioration. *Science* **332,** 1327–1330 (2011).
259 18. Padfield, D., Yvon-Durocher, G., Buckling, A., Jennings, S. & Yvon-Durocher, G. Rapid evolution
260 of metabolic traits explains thermal adaptation in phytoplankton. *Ecol Lett* **19,** 133–142 (2015).
261 19. Geider, R. J., Maclntyre, H. L. & Kana, T. M. A dynamic regulatory model of phytoplanktonic
262 acclimation to light, nutrients, and temperature. *Limnol. Oceanogr.* **43,** 679–694 (1998).
263 20. Raven, J. A. & Geider, R. J. Temperature and algal growth. *New Phytol* **110,** 441–461 (1988).
264 21. Toseland, A. *et al.* The impact of temperature on marine phytoplankton resource allocation and
265 metabolism. *Nature Climate Change* **3,** 979–984
266 22. Daines, S. J., Clark, J. R. & Lenton, T. M. Multiple environmental controls on phytoplankton growth
267 strategies determine adaptive responses of the N : P ratio. *Ecol Lett* **17,** 414–425 (2014).
268 23. Yvon-Durocher, G., Dossena, M., Trimmer, M., Woodward, G. & Allen, A. P. Temperature and the

biogeography of algal stoichiometry. *Global Ecology and Biogeography* **24,** 562–570 (2015).

24. Geider, R. & La Roche, J. Redfield revisited: variability of C:N:P in marine microalgae and its biochemical basis. *European Journal of Phycology* **37,** 1–17 (2002).
25. Dutkiewicz, S., Scott, J. R. & Follows, M. J. Winners and losers: Ecological and biogeochemical changes in a warming ocean. *Global Biogeochem. Cycles* **27,** 463–477 (2013).
26. Guillard, R. R. L. in *Culture of Marine Invertebrate Animals* 29–60 (Springer US, 1975). doi:10.1007/978-1-4615-8714-9_3
27. Schaum, C.-E. *et al.* Adaptation of phytoplankton to a decade of experimental warming linked to increased photosynthesis. *Nature Publishing Group* **1,** 1–7 (2017).
28. Amin, S. A. *et al.* Interaction and signalling between a cosmopolitan phytoplankton and associated bacteria. *Nature* **522,** 98–101 (2015).
29. Amin, S. A., Parker, M. S. & ARMBRUST, E. V. Interactions between Diatoms and Bacteria. *Microbiology and Molecular Biology Reviews* **76,** 667–684 (2012).
30. Brickley, M. R., Lawrie, E., Weise, V., Hawes, C. & Cobb, A. H. Use of a potentiometric vital dye to determine the effect of the herbicide bromoxynil octanoate on mitochondrial bioenenergetics in Chlamydomonas reinhardtii. *Pest. Manag. Sci.* **68,** 580–586 (2011).
31. Guzmán, H. M., la Jara Valido, de, A., Duarte, L. C. & Presmanes, K. F. Estimate by means of flow cytometry of variation in composition of fatty acids from Tetraselmis suecica in response to culture conditions. *Aquacult Int* **18,** 189–199 (2009).
32. Holm-Hansen, O. & Riemann, B. Chlorophyll a Determination: Improvements in Methodology. *Oikos* **30,** 438 (1978).
33. Murphy, J. & Riley, J. P. A modified single solution method for the determination of phosphate in natural waters. *Analytica Chimica Acta* **27,** 31–36 (1962).
34. Grasshoff, K., Kremling, K. & Ehrhardt, M. *Methods of seawater analysis*. (2009).
35. Suggett, D. J., Moore, C. M., Hickman, A. E. & Geider, R. J. Interpretation of fast repetition rate (FRR) fluorescence: signatures of phytoplankton community structure versus physiological state. *Mar. Ecol. Prog. Ser.* **376,** 1–19 (2009).
36. Falkowski, P. G., Dubinsky, Z. & Wyman, K. Growth-irradiance relationships in phytoplankton . *Limnol. Oceanogr.* **30,** 311–321 (1985).
37. Bowler, C. *et al.* The Phaeodactylum genome reveals the evolutionary history of diatom genomes. *Nature* **456,** 239–244 (2008).
38. Li, H. & Durbin, R. Fast and accurate short read alignment with Burrows-Wheeler transform. *Bioinformatics* **25,** 1754–1760 (2009).
39. Okonechnikov, K., Conesa, A. & García-Alcalde, F. Qualimap 2: advanced multi-sample quality control for high-throughput sequencing data. *Bioinformatics* (2015). doi:10.1093/bioinformatics/btv566/-/DC1
40. García-Alcalde, F. *et al.* Qualimap: evaluating next-generation sequencing alignment data. *Bioinformatics* **28,** 2678–2679 (2012).
41. Li, H. *et al.* The Sequence Alignment/Map format and SAMtools. *Bioinformatics* **25,** 2078–2079 (2009).
42. Cingolani, P. *et al.* A program for annotating and predicting the effects of single nucleotide polymorphisms, SnpEff. *Fly* **6,** 80–92 (2012).
43. Tibshirani, R., Hastie, T., Narasimhan, B. & Chu, G. Diagnosis of multiple cancer types by shrunken centroids of gene expression. *Proceedings of the National Academy of Sciences* **99,** 6567–6572 (2002).
44. Lê Cao, K.-A. *et al.* MixMC: A Multivariate Statistical Framework to Gain Insight into Microbial Communities. *PLoS ONE* **11,** e0160169–21 (2016).
45. Schoolfield, R. M., Sharpe, P. J. H. & Magnuson, C. E. Non-linear regression of biological temperature-dependent rate models based on absolute reaction-rate theory. *Journal of Theoretical Biology* **88,** 719–731 (1981).
46. Sharpe, P. J. & DeMichele, D. W. Reaction kinetics of poikilotherm development. *Journal of Theoretical Biology* **64,** 649–670 (1977).
47. Gillooly, J. F. Effects of Size and Temperature on Metabolic Rate. *Science* **293,** 2248–2251 (2001).
48. Brown, J. H., Gillooly, J. F., Allen, A. P., Van M Savage & West, G. B. Toward a metabolic theory of ecology. *Ecology* **85,** 1771–1789 (2004).
49. Van M Savage, Gillooly, J. F., Brown, J. H., West, G. B. & Charnov, E. L. Effects of Body Size and

Temperature on Population Growth. *The American Naturalist* **163,** 429–441 (2015).

50. Allen, A. P. Global Biodiversity, Biochemical Kinetics, and the Energetic-Equivalence Rule. *Science* **297,** 1545–1548 (2002).

Acknowledgments. This study was funded by a Leverhulme Trust research grant (RPG-2013-335). Whole genome re-sequencing was carried out at Exeter Sequencing Service and Computational core facilities at the University of Exeter, where Dr. Karen Moore, Dr. Audrey Farbos, Paul O'Neill and Dr. Konrad Paszkiewicz lead the handling of the samples. Exeter Squencing Services are supported by Medical Research Council Clinical Infrastructure award (MR/M008924/1), Wellcome Trust Institutional Strategic Support Fund (WT097835MF), Wellcome Trust Multi User Equipment Award (WT101650MA) and BBSRC LOLA award (BB/K003240/1).

Author contributions. GYD conceived and designed the study, analysed data and wrote the manuscript. ES designed and carried out the experimental work, analysed data and wrote the manuscript. AB conceived and designed the study. DS carried out the bioinformatic analyses of the genomic data. All authors contributed to writing the manuscript.

Author information. The authors declare no competing financial interests. Correspondence and requests for materials should be directed to ES or GYD.

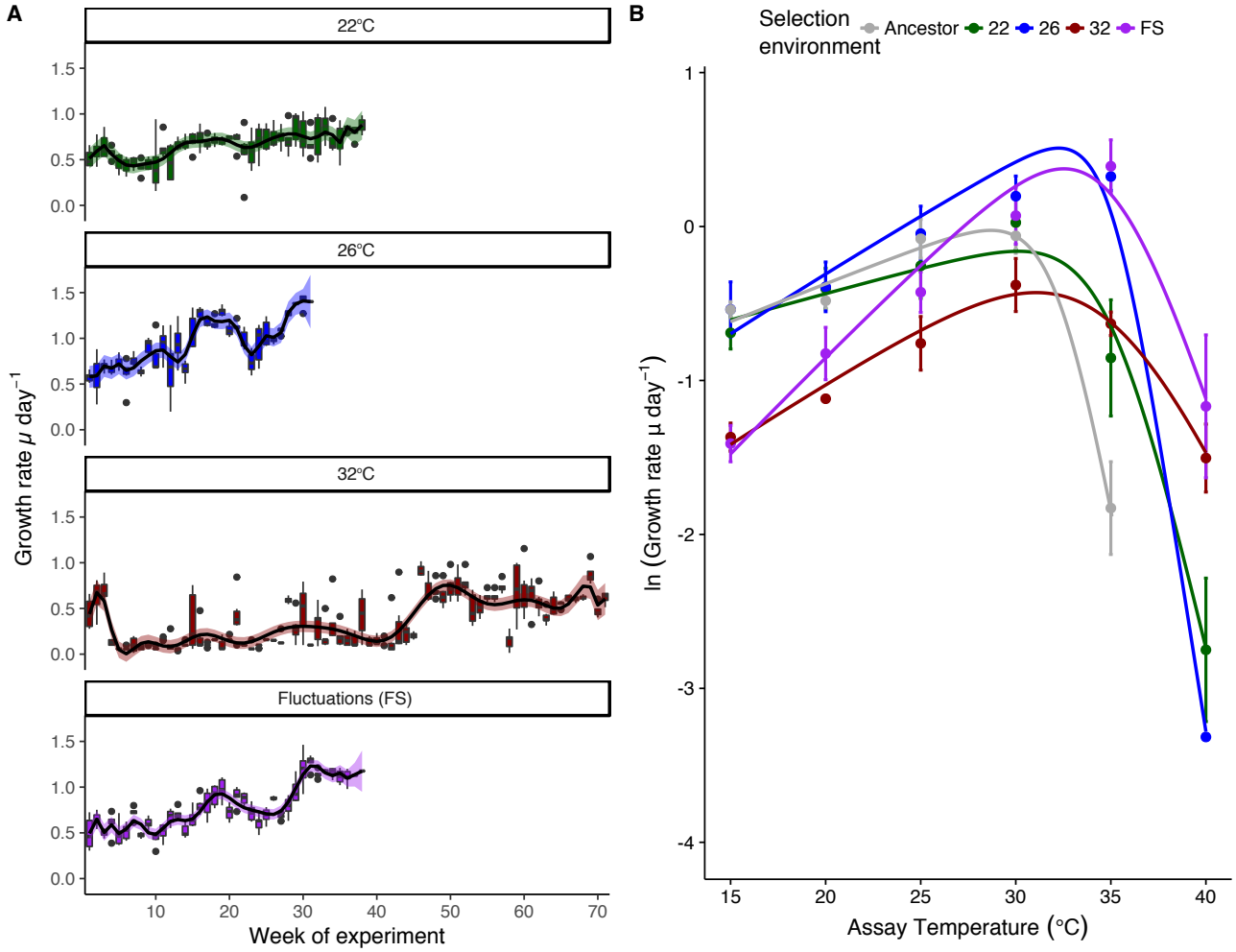

Figure 1| Growth rate trajectories and rapid evolutionary shifts in thermal tolerance curves. (A) Time-series of population growth rates reveal immediate and sustained increases in growth rates in populations adapting to moderate warming and the environment that fluctuated between 22 (benign conditions) and 32ºC (chronic conditions). In the 32ºC environment populations performed very poorly for approximately 1 year (~ 100 generation), followed by an evolutionary rescue event, which caused growth rates to increase to levels comparable with the control treatment at 22ºC. Boxplots were created by binning growth rate estimates across replicates on each week of the experiment until 300 generations had passed in each lineage. Fitted lines are from the best fits of a GAMM. **(B)** Thermal response curves of the ancestor and evolved lineages show marked shifts in thermal tolerance. Populations selected under moderate, severe and fluctuating warming all evolved increased tolerance of high temperatures relative to the ancestors and the control. Values are means and error bars denote ± 1s.e.m. Fitted lines are the fixed effects of a nonlinear mixed effects model. Grey curves denote the ancestor, green, samples are the control at 22ºC, blue is 26ºC, red is 32ºC, and purple is the fluctuating environment.

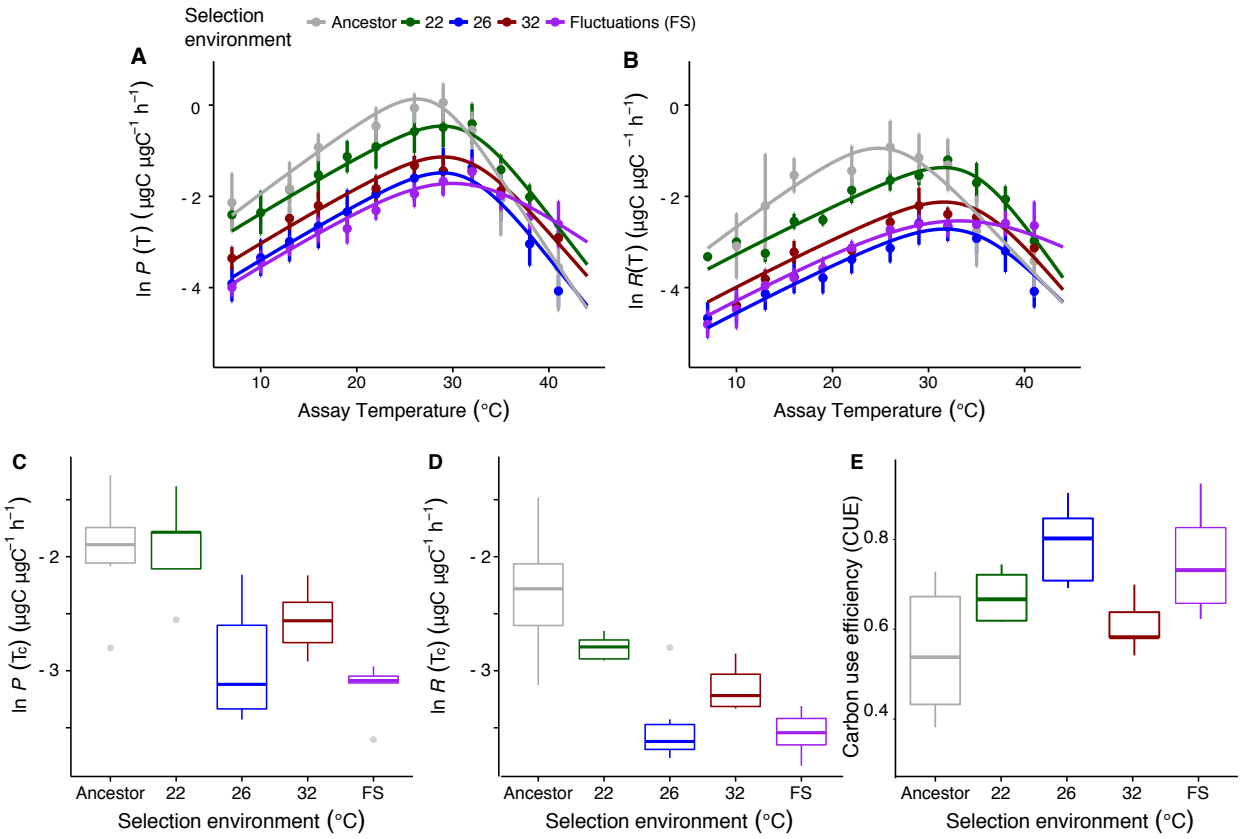

Figure 2| Rapid evolution of metabolic traits increase carbon-use efficiency. Thermal response curves for **(A)** gross photosynthesis rates (*P*), and (**B**) respiration (*R*) reveal substantial shifts in metabolic thermal traits both among treatments, as well as between the evolved lineages and the ancestor. Data are presented as means with error bars denoting ± 1s.e.m, $n = 6$ per assay temperature, fitted lines are fixed effects from non-linear mixed effects models. Mass-specific rates of (**B**) gross photosynthesis and (**C**) respiration normalized to reference temperature ($P(T_c)$ and $R(T_c)$ respectively, see methods) were significantly down-regulated in the populations evolved under moderate, chronic and fluctuating warming. Furthermore, rates of $R(T_c)$ were down-regulated more than those of $P(T_c)$ in the moderate and fluctuating warming treatments resulted in high meaning that (**C**) those lineages also had the highest carbon-use efficiency (CUE). Grey denotes the ancestor, green is the control at 22ºC, blue is 26ºC, red is 32ºC, and purple is the fluctuating environment. Carbon use efficiency for FS is displayed at 32ºC for easier comparison to the 32ºC-evolved samples, and did not differ significantly between assay temperatures of 22ºC, 26ºC, and 32ºC (see also Figure S3).

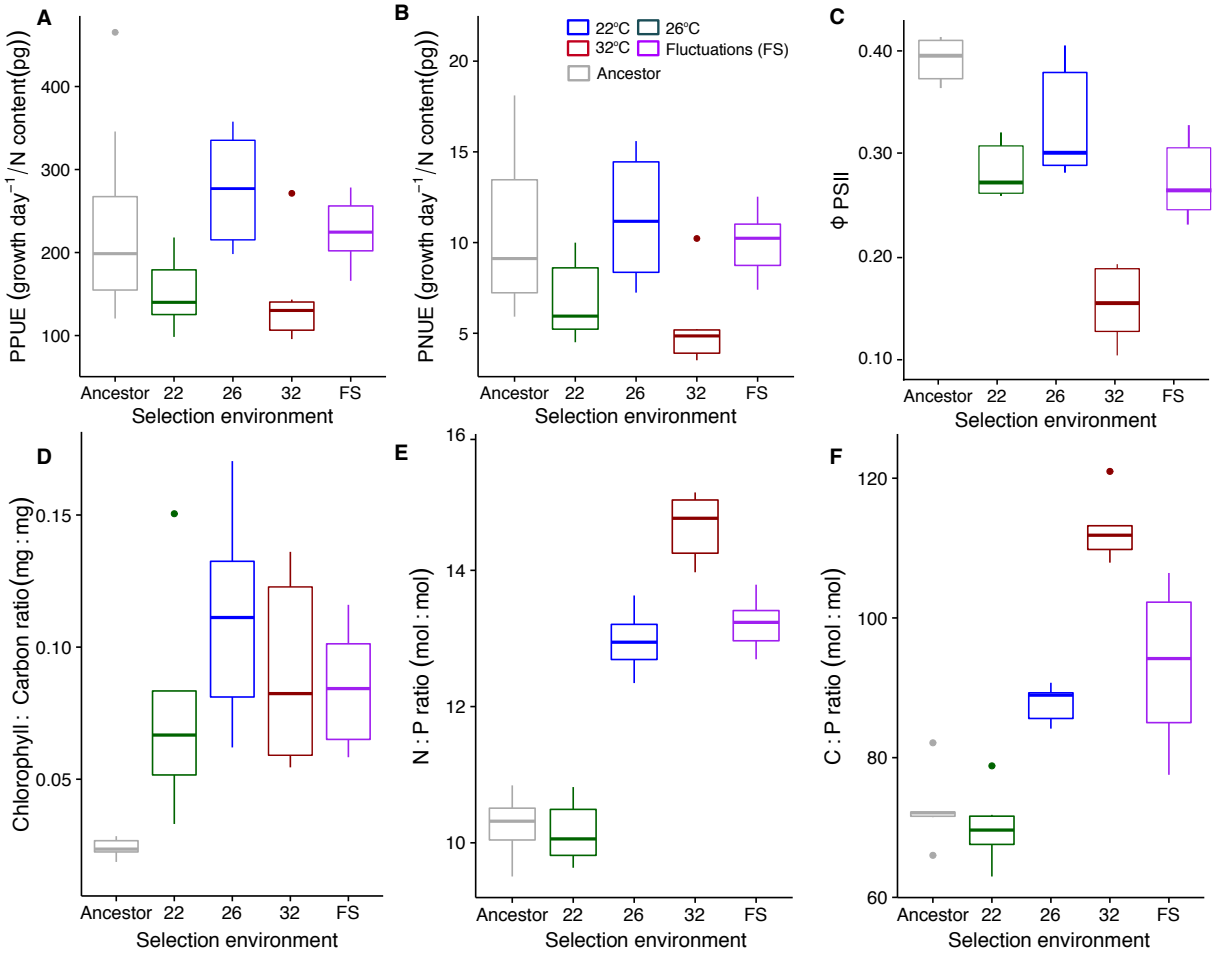

Figure 3 | Evolutionary shifts in macromolecular composition, photosynthetic and nutrient-use efficiency. (**A**) the phosphorous-use efficiency (**B**) the nitrogen-use efficiency and (**C**) the quantum efficiency of photosystem II (Φ_{PSII}) were highest in the fastest growing lineages selected under moderate and fluctuating warming and showed a similar pattern among treatments to variation in metabolic efficiency (e.g. ε in Fig. 3). (**D**) The chlorophyll-to-carbon ratio was also highest in the fastest growing lineages selected under moderate warming. (**E**) The N:P and (**F**) the C:P ratios increased with increasing selection temperature, with values in the fluctuating environment comparable to those in the moderate warming treatment. For all panels, $n = 6$. Boxplots are for the ancestor (grey) and evolved lineages after 300 generations at 22 ºC (green), 26ºC (blue), 32ºC (red) and the fluctuating environment (purple). Values for the ancestor are as measured at 22ºC. See also Fig. S3 for additional phenotypic trait values.

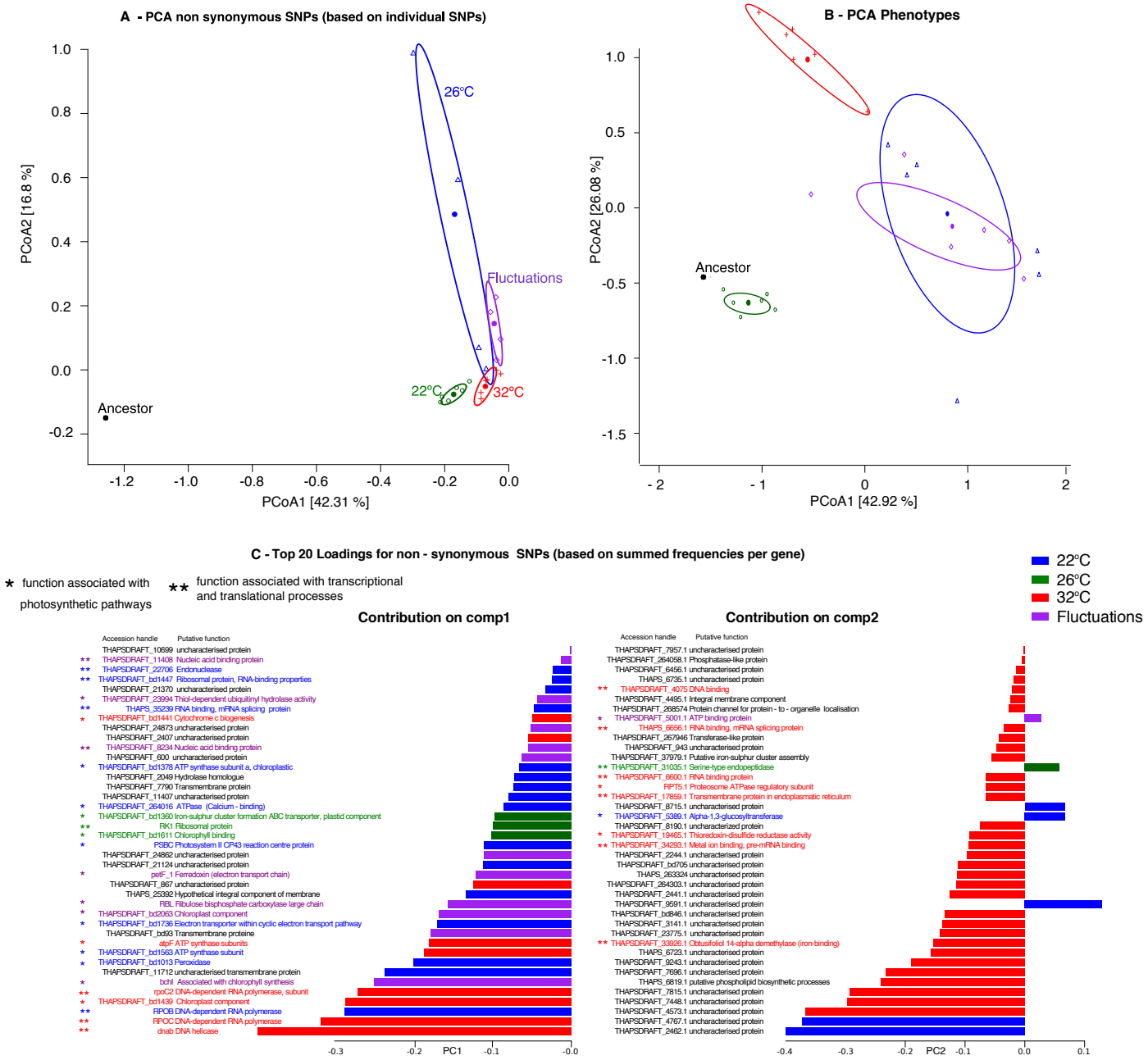

Figure 4 | Phenotypic and molecular evolution in *T. pseudonana*. (A) Principal components analysis (PCA) of evolved and ancestral lineages calculated from the frequency and identity of non-synonymous SNPs. (B) PCA of phenotypic traits calculated from the change in each trait measured at the treatment temperature relative to that expressed in the ancestor at the same temperature (C) The top 20 genes most strongly associated with each of the treatments derived from the first two principal components.

401
402 **METHODS**

403 Experimental Design

404 The sequenced strain of *Thalassiosira pseudonana* (CCMP 1335)[11] was obtained from the CCAP
405 culture collection in November 2014. The stock culture was made clonal by serial dilution in a
406 96-well plate in March 2015 and a single clone was chosen at random to be the ancestor for all
407 treatments in the selection experiment. Pilot experiments with the ancestor revealed that growth
408 rates peaked at 28ºC and were negative above 35ºC. The ancestor was then distributed among 4
409 experimental treatments that represent a range of warming scenarios based on its limits of
410 thermal tolerance: (i) a control at 22ºC, which was the long-term culture temperature; (ii)
411 moderate warming at 26ºC; (iii) severe warming at 32ºC and (iv) a fluctuating thermal regime,
412 which cycled between 22 and 32ºC every 3-4 generations. Each treatment was replicated 6
413 times.

414 Lineages were grown in grown in f/2 Medium (Guillard's medium for diatoms[26]) with
415 artificial seawater, under a 12:12 light/dark cycle. Salinity was maintained at 32 (i.e. 32g NaCl L^{-1}
416 in 39.5 g L^{-1} artificial seawater reagents) and pH adjusted to 8.213 ± 0.291 (± s.e.m., averaged
417 across all transfers) prior to each transfer. pH was further measured at the end of each transfer
418 (average across all transfers: 8.171 ± 0.252). Light intensity was at 100 µmol quanta m^{-2} s^{-1}.
419 Lineages were maintained in semi-continuous batch culture, and transferred during the
420 exponential phase of growth to an inoculum of 100 cells mL^{-1}. This minimizes demographic
421 effects that arise by slow-growing populations going through bottle-necks where mutational
422 supply is limited to a point at which adaptive potential is determined by population size alone,
423 but still allows for population size, and hence mutational supply to play a crucial role in shaping

424 evolutionary trajectories, as faster growing lineages will receive on average more diverse
425 inocula.
426
427 Flow cytometry
428 Abundance and cell size (diameter assuming a spherical shape) were determined with a Accuri
429 C6 flow cytometer (BD Scientific). Cell size was detected using forward scatter (FSC) calibrated
430 using species and beads of known size against photographic images processed in ImageJ as
431 described in[27], with a conversion factor of FSC=108058 µm + 4.5665. Although *T. pseudonana*
432 are cylindrical rather than spherical, this is a useful approximation for relative changes in cell
433 size. Red fluorescence (FL3) was used for chlorophyll fluorescence in order to distinguish
434 autotrophs from bacteria, but was not used here to approximate chlorophyll content, which was
435 instead estimated through acetone extraction (see below). Co-occuring bacteria, e.g. *Rhodobacter*
436 *spp* and *Marinobacter spp* are known to be crucial for nutrient recycling and signaling molecule
437 metabolism in *T. pseudonana*[28,29]. We therefore made no attempt to make the cultures axenic as
438 this would have incurred a substantial fitness cost. We quantified the associated bacteria by
439 regularly filtering the cultures between 0.2µm to 2µm, staining with SYBR gold and
440 enumerating bacterial densities and cell size via flow cytometry. Co-occurring bacteria
441 contributed less than 1% of total biomass.

442 Flow cytometry was further used in combination with a rhodamine stain to measure a
443 proxy for mitochondrial potential – the rate of ATP production by ATP synthase is proportional
444 to mitochondrial potential, which in turn depends on the activity of respiratory proteins
445 embedded in the mitochondrial membrane. Since each unit area of membrane has a number of
446 ATP synthase molecules and the rate at which each of these produces ATP depends on the

447 mitochondrial potential, the overall rate of ATP production per mitochondria depends on both
448 the area of mitochondrial membrane and the mitochondrial potential. Mitochondrial area is a
449 good approximation of the area of mitochondrial membrane, and changes in mitochondrial
450 potential can be measured in live cells using potentiometric dye. Previous work[30] has shown that
451 the styrl dye rhodamine 123 (R123) can be used in live cells of phytoplankton to measure
452 mitochondrial potential in real time. For staining, a 10 mg mL^{-1} stock solution in DMSO was
453 prepared and diluted to a 1µM working solution on the day of measurements. Of this, 20 µL
454 were added to 200 µL of sample and left to incubate in the dark for 45 minutes. To ensure that
455 longer incubation as is inevitable on a 96 well plate did not effect FL1 fluorescence as measured
456 in the accuri c6, samples were randomized across each 96-well plates with the first and the last
457 well containing the same sample. We found no effect of prolonged incubation after an incubation
458 period of 45 minutes.

459 A Nile Red stain was performed to measure relative lipid contents. Here, the dye was
460 used as a proxy to determine relative quantities of intracellular polar and neutral lipids[31] in
461 evolved samples, and in samples from short-term assays. The stock dye was obtained as a
462 powder. The working solution was diluted to 0.1 mg L^{-1}, and 10 µL were added to each 200 µL
463 sample on a 9-well plate (final concentration 15 mM) and left to incubate in the dark for 30
464 minutes, as pilot trials had shown that after this, fluorescence levels were stable long enough for
465 the time taken to measure one 96 well plate. Samples were randomized on the plate as described
466 above for R123 stains. As Nile Red excites in the same wavelength as chlorophyll (FL3) and
467 chlorophyll derivatives (FL2), samples were measured before and after adding the dye, and the
468 chlorophyll fluorescence subtracted from the fluorescence obtained after staining the sample.

469

Growth rate trajectories

At the beginning and at the end of each transfer *T. pseudonana* cells were counted on the flow cytometer as described above and used to estimate specific growth rates (μ d^{-1})

$$\mu = \frac{\ln(N_{t1}) - \ln(N_{t0})}{\Delta t} \quad (1)$$

where N_{t1} is the density of cells at the end of the transfer, N_{t0} is the inoculation density, and Δt is the time passed in days.

Thermal tolerance curves

To characterize the thermal tolerance curves of the ancestor and each of the evolved lineages, an inoculum of 100 cells per mL from the middle of the logarithmic phase of growth was transferred into fresh media at 15ºC, 20ºC, 25ºC, 30ºC, 32ºC, 35ºC, and 40ºC. Cell count was then determined daily on a flow cytometer and populations were transferred to fresh media once at each temperature during the middle of the logarithmic phase of growth, before being left to reach stationary phase. Growth rates were estimate from the abundance data using a the logistic growth function

$$N(t) = \frac{K}{1 + \frac{K - N_{t0}}{N_{t0}} e^{rt}} \quad (2)$$

where t is time, K is carrying capacity of the population (cell mL^{-1}), r is the maximum growth rate (d^{-1}) and N_{t0} is the cell count at t_0 (cell mL^{-1}).

489

490 Intracellular macromolecular composition

491 Cellular carbon (C), nitrogen (N), phosphorous (P) and chlorophyll content (total chlorophyll
492 calculated from chlorophyll *a* and chlorophyll *c* content) were quantified in the ancestor and each
493 of the evolved lineages. We investigated the effects of temperature on macromolecular
494 composition both over short-term acclimation and long-term evolutionary adaptation. Short-term
495 thermal acclimation was investigated by exposing the evolved lineages to the 15 to 45ºC thermal
496 gradient described above for quantifying the thermal tolerance curves for growth rate. Here,
497 lineages were given 1 transfer to acclimate to a given assay temperature in the gradient and then
498 harvested during the logarithmic phase of growth in the second transfer. Long-term evolutionary
499 adaptation to the selection regimes was quantified by harvesting evolved lineages directly from
500 the experiment during the logarithmic phase of growth.

501 The samples were prepared for C, N, P and chlorophyll measurement by spinning down
502 50 mL of culture in a centrifuge at 4ºC and 3500RPM for 30 minutes. The pellet was then
503 transferred to a 1 mL Eppendorf tube, spun again for 15 minutes at 3500RPM and the remaining
504 supernatant decanted. Chlorophyll content was determined on a spectrophotometer (Jenway
505 7351) after[32], with extraction in 100% methanol, and absorption spectra measured in 10 nm
506 increments from 500 to 700nm, which span the full range of emission peaks for chlorophyll a
507 and chlorophyll c.

508 Pellets for C and N determination were freeze dried for 24 hours, transferred to zinc
509 capsules, weighed and analyzed using a SerCon Isotope Ratio Mass Spectrometer (CF-IRMS)
510 system (continuous flow mode). Intracellular P content was determined was determined via a
511 colourimetric reaction on a Seal Analytics AA3 segmented flow auto-analyzer. Freeze dried

pellets were washed in 0.17M Na_2SO_4, transferred to scintillation vials and re-suspended in 4 ml 0.017M $MnSO_4$. The samples were transferred to an autoclave (1h, 121ºC), shaken vigorously and centrifuged at 2500 r.p.m for 30 minutes, the pellet discarded, and the supernatant brought to 10 ml with MillliQ purified water. The samples were immediately analyzed on the AA3 using the colourimetric molybdate/antimony method[33]. Using these data we calculated the molar stoichiometric ratios, C:N, C:P, N:P and the Chl:C ratio. Nitrogen-use efficiency (PNUE) and phosphorous-use efficiency (PPUE) were characterized as the ratio of growth rate to cellular nutrient concentration in pg.

Silica content, although not a main trait under investigation here, was determined through preparing pellets as described above. Then, 4ml of 0.2M NaOH were added to the pellet in polyethylene tubes and the pellets vortexed briefly. The samples were then transferred to a heating block at 90ºC for ca. 1h. 2 ml of 1M HCl were added, the samples vortexed again and then spun at 3500 rpm for 1h. The supernatant was passed through an 0.5µm filter, pipetted into fresh tubes, topped up to 10ml with MiliQ water and used immediately on the segmented flow auto-analyser, where the colourimetric procedure followed that described in[34].

Photochemistry

We characterised a range of photochemical parameters in the ancestor and each of the evolved lineages using fast repetition rate fluorometry (FastPro8, FRRf3, Fast Ocean System Chelsea Technology Group). 500 µL of dilute sample (with a cell count of less than 1000 cells mL^{-1}) were added to 5 ml of fresh culture medium. Samples were then pre-incubated in the dark at the assay temperature for 15 minutes in a water-bath, and another 10 minutes in the fluorometer to make sure that samples were fully dark acclimated and all reaction centers closed. All

535 measurements were made at the selection temperature for the 22, 26, and 32ºC lineages, while
536 for the lineages in the fluctuating regime measurements were carried out at both 22 and 32ºC.
537 Photochemical traits were measured in response to rapid flashes at increasing light intensities
538 from 0 to1600 µmol m^{-2} s^{-1}. Flash frequency and rate followed standard protocols for
539 phytoplankton[35], with 100 flashes of 1.1 µs at 1 µs intervals. Peak emission wavelengths of the
540 LEDs used for excitations were at 450 nm, 530 nm, and 624 nm. Φ_{PSII} was particularly relevant
541 to our study as it is commonly used to describe the light responses of photosynthetic efficiency.
542 Φ_{PSII} values are used as an indication of the proportion of the total light absorbed that is used in
543 photochemical reactions in PSII (see also Table S10 and Figure S3). Additionally, we
544 determined rP, NPQ, and *C* (see Fig. 4B and SI Table 13 for PCA on phenotypic traits). These
545 describe the relative rate of photosynthesis in response to irradiance and are obtained as an
546 estimate of electron transport through PSII (rP), the cell's ability to maintain photochemical
547 function at high light intensities (NPQ, non photochemical quenching) and the proportion of PSII
548 reaction centers in a closed state (*C*). As measurements were carried out following a light
549 response curve, we were then able to measure these functions both at saturating light intensity
550 and at the light intensity that the samples were grown at in the incubators.
551

552 Thermal responses of photosynthesis and respiration
553 Measurements of photosynthesis and respiration were made on the ancestor and all evolved
554 lineages after 300 generations of selection when in the middle of the logarithmic phase of
555 population growth. Net photosynthesis (*NP*) was measured as O_2 evolution at increasing light
556 intensities in intervals of 50 µmol^{-1} m^{-2} s^{-1} up to 300 µmol^{-1} m^{-2} s^{-1}, and then in intervals of 100
557 µmol^{-1} m^{-2} s^{-1} up to 1000 µmol^{-1} m^{-2} s^{-1}, followed by 200 µmol steps up to 2000 µmol^{-1} m^{-2} s^{-1}.

The maximum rate of light saturated photosynthesis was determined by fitting the *NP* data to a dynamic model of photoinhibition via non-linear least squares regression using the methods outlined in[18]:

$$NP(I) = \frac{NP_{max} I}{\frac{NP_{max}}{\alpha I_{opt}^2} I^2 + \left(1 - 2\frac{NP_{max}}{\alpha I_{opt}}\right) I + \frac{NP_{max}}{\alpha}} - R \quad (3)$$

where $NP(I)$ is the rate of photosynthesis at light intensity I, NP_{max} is the maximum rate of net photosynthesis at the optimal light intensity, I_{opt}, and α controls the rate at which $NP(I)$ increases up to NP_{max} and R is the rate of respiration (i.e. the rate of O_2 flux when $I = 0$). Gross photosynthesis (P) was estimated as $P = NP_{max} + R$. Measurements of O_2 flux were measured in a Clark-type oxygen electrode (Hansatech Ltd, King's Lynn UK Chlorolab2). Aliquots (50 mL) of the populations were concentrated through centrifugation to a density of approximately $8*10^4$ cells mL^{-1} and acclimatised to the assay temperature for 15 minutes in the dark before measuring metabolic rates. The thermal responses of P and R were quantified by measuring rates over a temperature gradient from 4ºC to 45ºC (in 3ºC increments, with additional measurements at the selection temperatures). Rates of P and R were expressed in units of µg C per µg C using the following equation [36]

$$b(\mu gC\ \mu gC^{-1}) = \frac{b(\mu mol\ O_2\ mL^{-1}\ d^{-1} * 32 * M * (\frac{12}{44}))}{\mu mol\ C\ cell^{-1} * cells\ mL^{-1}} \quad (4)$$

where b is the metabolic rate (either P or R), $32 * M * (12/44)$ is used to convert µmol O_2 into µg C, and the factor M, is the assimilation quotient of CO_2:O_2. In our study, NO_3^- was the source of nitrogen, thus assuming a set of balanced growth equations[36]:

$$nCO_2 + (n+1)H_2O + HNO_3 \rightarrow (CH_2O)_n NH_3 + (n+2)O_2 \quad (5)$$

579 if the C:N ratio is calculated in moles the assimilation ratio of CO_2:O_2 will be n/n+2 (see[36]). The
580 estimated *M* values are given in Table S1 and ranged from ~ 0.77 to ~ 0.79. Alongside the
581 biomass measurements for phytoplankton, we also periodically measured bacterial biomass (see
582 methods detailed above), which typically comprised <1% of algal biomass. Consequently,
583 bacterial respiration did not contribute significantly to metabolic rates, and when 2µm filtered
584 samples were run for metabolic rate measurements, the slopes were indistinguishable from water
585 blanks.

586

587 DNA extraction for Whole Genome Re-Sequencing

588 At the beginning (t000) and after 300 generations (t300) of selection in each environment, 250ml
589 of each sample in exponential growth were spun to a pellet in 50ml batches at 4ºC and 3500
590 RPM (rounds per minute). The supernatant was discarded and the pellet stored at -20ºC until
591 further use. Prior to DNA-extraction, samples were put through three cycles of thawing and
592 refreezing, as this had shown to increase yield of diatom DNA relative to bacterial DNA in pilot
593 studies. DNA was extracted following a standard cTAB protocol in chloroform:isoamyl and
594 isopropanol (Murray and Thompson, 1980) with a proteinase K step to digest proteins, and an
595 RNAse step to digest RNA. The resulting DNA pellet was quality controlled on 1% agarose gels
596 and fluorometrically on a Qbit system. The extracted genomic DNA was then frozen in TE
597 buffer at -20ºC until samples were processed at the Exeter Sequencing Services (University of
598 Exeter, UK). Whole genome re-sequencing (Illumina) was carried out on a HiSeq 2500 platform
599 with paired-end reads. Library preparation was carried out at the Exeter Sequencing Services
600 using Netflex. The resulting reads were assembled against the existing *T. pseudonana* genome [11].
601 Quality control filtering of sequence data

We generated paired 125-bp reads from genomic DNA from 61 samples (plus three negative controls containing no diatoms) using the Illumina HiSeq. Reads were trimmed and filtered to remove poor quality data using Trimgalore (https://www.bioinformatics.babraham.ac.uk/projects/trim_galore/) with "–q 30".

Variant calling: single-nucleotide polymorphisms (SNPs)

After trimming and filtering, remaining sequence reads were then aligned against version 2 of the reference *T. pseudonana* genome sequence [11,37] (GenBank: GCA_000149405.2) using BWA-mem version 0.7.5a-2 with default settings [38]. Alignment statistics were calculated using Qualimap [39-41].This resulted in average aligned sequence depths from 3.4 to 74.5 fold; the average alignment depth for the t0 (ancestor) sample was 18.5 fold. This resulted in a set of 64 BAM-formatted [41] files (see also Table S15).

Each BAM file was converted to *mpileup* format using SAMtools [41] version 0.1.19-1. The *mpileup* file contains, for each position in the alignment, the frequency of each base (allele) among the sequence reads aligned at that position; in other words it offers an estimate of the frequencies of each allele among the sequenced population. We considered only those genomic positions that in the t0 (ancestor) sample had a single base (*i.e.* allele) with a 100 % frequency; in other words we excluded from consideration genomic sites where there was ambiguity about the genetic state in the ancestor population. SNP sites falling within protein-coding exons were classified as synonymous or non-synonymous using the SNPeff tool [42].

We combined the allele frequencies from each *mpileup* file into a single matrix, which was used for the downstream statistical analyses implemented in R using the packages vegan (2.4-3), mixOmics (6.1-3), and phangorn (2.2-0). Specifically, we created distance matrices on

625 which we ran PERMANOVAs to test for separation of samples (on phenotypic data and SNPs)
626 by treatment. Pairwise contrasts between treatments were examined in PERMDISP followed by
627 TukeyHSD post-hoc tests. Trees were built within the phangorn package through neighbour-
628 joining, and annotation of trees was carried out in the FigTree software (FIGTREE 1.4.3
629 http://tree.bio.ed.ac.uk/software/figtree/).

630 To visualise treatment associated PCA-loadings, we used the plotLoadings functions
631 within the mixOmics package, which performs discriminant PCA and then represent the loading
632 weight of each selected variable on each component, i.e. the length of the bar is directly
633 correlated to the location of the loadings on the PCA, with the longest bar indicating the
634 strongest association to a treatment group. This allows us to find treatment associated groups in
635 which the changes in the selected gene or SNPs are maximal [43,44].

636

637 Statistical Analyses

638 *Fitness trajectories*

639 The resultant time series of specific growth rates were analyzed using a generalised additive
640 mixed effects model (GAMM) to assess whether the fitness trajectories differed between the
641 selection regimes. We used GAMMs to account for the hierarchical nature of our experimental
642 data. For example, our experimental design yielded replicate fitness trajectories in each selection
643 treatment. This hierarchical structure meant that measurements were non-independent – e.g.
644 measurements from the same replicate will be auto correlated. We account for this by treating
645 replicate as a random effect on the intercept of the model, which models deviations among
646 replicates from the fixed effects as normally distributed with a mean of zero. The most complex
647 models included an effect of treatment (e.g. '22', '26', '32', '22-32') on the intercept (which

characterises the median value of the response variable) and also allowed the shape of the time series, which was modeled using a cubic regression spline, to vary among treatments. Treatment effects on the shape and intercept of the seasonal phenology were modeled as fixed effects in the GAMMs. Model selection entailed fitting a range of models to the data, starting with the full model and then a series of reduced models with interaction terms and main effects removed to test hypotheses about the potential differences in the fitness trajectories among treatments. For multi-model selection we computed small sample-size corrected AIC scores (AICc) and then compared between models by calculating delta AICc values and AIC weights using the 'MuMIn' package. GAMMs were fitted to the data using the 'gamm4' package and were conducted in R (v.3.23).

Thermal responses of growth and metabolism

The thermal responses for growth, photosynthesis and respiration were quantified using a modified version of the Sharpe-Schoolfield equation (see[45,46] for the original equations), which assumes that the rate of growth or metabolism is limited by single enzyme catalyzed reaction

$$\ln\big(b(T)\big) = E_a\left(\frac{1}{kT_c} - \frac{1}{kT}\right) + \ln\big(b(T_c)\big) - \ln\left(1 + e^{E_h\left(\frac{1}{kT_h} - \frac{1}{kT}\right)}\right) \quad (6)$$

where $b(T)$, is the rate of metabolism (in µg C µg C^{-1} d^{-1}) or growth (d^{-1}), k is Boltzmann's constant (8.62×10^{-5} eV K^{-1}), E_a is the activation energy (in eV) for the metabolic process, indicative of the steepness of the slope leading to a thermal optimum, T is temperature in Kelvin (K), E_h characterises temperature-induced inactivation of enzyme kinetics above T_h where half the enzymes are rendered non-functional and $b(T_c)$ is the rate of metabolism normalised to an

arbitrary reference temperature, here T_c = 18ºC, where no low or high temperature inactivation is experienced. Equation (6) yields a maximum metabolic rate at an optimum temperature, where metabolic rates are fastest:

$$T_{opt} = \frac{E_h T_h}{E_h + kT_h \ln\left(\frac{E_h}{E_a} - 1\right)} \quad (7)$$

Equation (6) differs from the Sharpe-Schoolfield equations in a number of ways. First, we exclude parameters from Eq. (6) used to characterise low-temperature inactivation due to insufficient data to quantify this phenomenon in our analysis. Second, rather than characterise temperature effects below T_{opt} using the Eyring (1935) relation, $\left(\frac{T}{T_c}\right) e^{E_a\left(\frac{1}{kT_c} - \frac{1}{kT}\right)}$, we instead use the simpler Boltzmann factor, $e^{E_a\left(\frac{1}{kT_c} - \frac{1}{kT}\right)}$. This simplification enables an explicit solution for T_{opt} (Eq. 8) and facilitates more direct comparison with previous work on the temperature dependence of metabolism using metabolic theory[47-50] .

The parameters $b(T_c)$, E_a, E_h, T_h, and T_{opt}, represent traits that characterise a unimodal thermal response curve, and we expect them to differ between selection regimes owing to thermal adaptation. To test this hypothesis, we fitted the rate data to Eq. (6) using non-linear mixed effects models in the 'nlme' package in R. We analyzed the photosynthesis, respiration and growth data in separate mixed effects models. We also analyzed the thermal responses for ancestor separately from the data for the evolved lineages following the selection experiment. Models included random effects on each of the parameters of Eq. (6) by replicate, and for the analysis with evolved lineages, 'selection environment' as a fixed four level factor on each parameter. For the analysis of the metabolism data for the ancestor we included both photosynthesis and respiration data together, with 'flux' as a two-level fixed factor on each of the

parameters in Eq. (6), to establish whether the thermal responses differed between these fluxes and likely physiological constraints on growth prior to the selection experiment. Model fitting and selection started with the most complex possible model, including fixed and random effects on all parameters. Model selection then proceeded by first removing treatment effects on the parameters individually, then in pairs of two and in pairs of three, and finally, by removing the treatment-effect all four parameters. For multi-model selection we computed small sample-size corrected AIC scores (AICc) and then compared between models by calculating delta AICc values and AIC weights using the 'MuMIn' package. When candidate models deviated from the most parsimonious model (that with the lowest AICc score) by less than two AICc units, parameters were averaged across those candidate models. The relative importance of the fixed factors in the averaged model was determined using the sum of their relative weights (see Table S5 and S6).

Carbon-use efficiency (CUE)

Carbon use efficiency, as the *potential* for carbon allocation to growth, was calculated from the gross photosynthesis (P) and respiration (R) data as $\mathrm{CUE} = 1 - R/P$. For statistical analysis, we used CUE calculated at the temperature of the selection environment. In the fluctuating treatment, we used data for photosynthesis and respiration at 32ºC to aid comparison with the populations experiencing 32ºC throughout. We fitted a linear mixed effects model to these data, with 'selection regime' as a fixed effect and biological replicate as a random effect. Model selection proceeded as described above.

712 *Macromolecular composition and photosynthetic efficiency*

713 The C, N and P content, the C:N, C:P, N:P, Chl:C ratio, size and silicate content, as well as Φ_{PSII}
714 at high and low light, were each analyzed using a separate mixed effects model, where 'selection
715 regime' was a fixed effect and replicate was a random effect on the intercept (see Table S11 for
716 details). Model selection was as described above.

717 We quantified the light response curve of Φ_{PSII} using an exponential decay model

718 $$\Phi_{PSII} = a * \exp(I * b) \quad (8)$$

719 where I is the irradiance, a is a normalization constant, and b is the rate constant which
720 characterises how rapidly Φ_{PSII} declines with increasing I. Eq. (8) was fitted to the Φ_{PSII} data
721 using a non-linear mixed model including random effects by biological replicate on each
722 parameter and 'selection environment' as a fixed factor. Model output was then used to calculate
723 Φ_{PSII} at the light intensity that samples would have experienced in the incubators (i.e. ~ 100µmol
724 quanta m^{-2} s^{-1} see Fig. 4 G). Model selection then proceeded as described above for P and R data.
725 Detailed model output and model selection data are available in Table S10 where nomenclature
726 and acronyms are as given here (see also Figure S4).
727